

Thermodynamic, pyrolytic, and kinetic investigation on the thermal decomposition of polyvinyl chloride in the presence of franklinite

Sanad Altarawneh^{a,*}, Mohammad Al-Harabsheh^b, Chris Dodds^a, Adam Buttress^a, Sam Kingman^a

^a Faculty of Engineering, University of Nottingham, Nottingham NG7 2RD, UK

^b Chemical Engineering Department, Jordan University of Science and Technology, Irbid 22110, Jordan

ARTICLE INFO

Keywords:

Non-isothermal kinetics
Zinc iron oxide
TGA
Activation energy
EAFD
PVC

ABSTRACT

Thermal co-treatment of Electric Arc Furnace Dust (EAFD) and polyvinyl chloride (PVC) may provide a viable route for reprocessing these hazardous materials within the circular economy. To develop and optimise a commercial treatment process, the complex mechanistic pathway resulting from the reaction of these two wastes must be understood. Franklinite (ZnFe_2O_4) is a major zinc containing phase in EAFD and to date, little work has been undertaken on the decomposition of PVC in its presence. Herein, we present a thermodynamic, pyrolytic, and kinetic study of PVC degradation in the presence of ZnFe_2O_4 . It was found that ZnFe_2O_4 decomposed to its associated halides. Additionally, the kinetics data confirmed the catalytic activity of ZnFe_2O_4 , dropping the dehydrochlorination onset temperature of PVC from 272 to 235 °C. The distribution of the activation energy with conversion suggests the presence of several competitive reactions each with a different energy barrier. In such a case, reaction channelling can take place leading to selective zinc chlorination. Moreover, since the reduction of Fe_2O_3 is slow at low temperatures, it is recommended to operate at a temperature as low as 235 °C which can promote the chlorination selectivity towards zinc leaving iron bearing compounds in their stable form (Fe_2O_3).

1. Introduction

During steel manufacturing, hazardous electric arc furnace dust (EAFD) is generated as a waste by-product. About 7.5 million tons of EAFD is globally produced annually from steel manufacturing (Teo et al., 2018). The chemistry of the generated EAFD strongly depends on the quality of the scrap being employed in the smelting and the composition of other input materials (KiranKumar and Roy, 2022). Despite the variation in EAFD chemistry, the presence of toxic heavy metals such as Pb and Cd has been reported (Al-Harabsheh, 2017; Laubertova et al., 2020). Hence, the large production rate of this material along with the toxic nature of some of its constituents, poses a huge environmental threat. This, in turn, puts a huge pressure on steel manufacturers who resort to landfilling as their major disposal strategy.

Aside to landfilling, the scientific community has directed significant endeavour towards the utilisation of EAFD as a source of zinc by means of hydrometallurgical (Al-Makhadmeh et al., 2018; Laubertova et al., 2020; Oustadakis et al., 2010; Teo et al., 2018) and pyrometallurgical (Omran et al., 2019; Sinaga et al., 2019; Ye et al., 2020; Zhang et al.,

2019) treatment routes. Currently, the latter has reached an industrial level. About 83% of EAFD is recycled in the Waelz kiln process (Yakornov et al., 2017). However, the pyrometallurgical approach is only capable of increasing the zinc concentration in EAFD (zinc enrichment) by means of volatilisation, oxidation, and then collection without a complete separation of the metal at a high purity. The furnace utilised in the Waelz process also operates at a temperature of 1200 °C (Suetens et al., 2014) which makes this process highly energy intensive. Industrial uptake of hydrometallurgical treatment methods, in contrast, is limited due to the resistive nature of franklinite (ZnFe_2O_4) which prevents the complete extraction of zinc and highlights the importance of rejecting iron from the leaching liquor when acidic reagents are used.

Plastics are also accumulated in large quantities. Polyvinyl chloride (PVC) is a versatile thermoplastic and is classified an industrial polymer with high importance (Marcilla and Beltrán, 1995). PVC is ranked the third (after polypropylene and high and low density Polyethylene) in terms of converters plastic demand in Europe at 4.7 million tons in 2020 (Plastics-Europe, 2021). This could be assigned to the superior properties and the high versatility of this material. Nonetheless, PVC is

* Corresponding author.

E-mail address: sanad.altarawneh@nottingham.ac.uk (S. Altarawneh).

<https://doi.org/10.1016/j.psep.2022.10.028>

Received 4 July 2022; Received in revised form 8 October 2022; Accepted 12 October 2022

Available online 14 October 2022

0957-5820/© 2022 The Author(s). Published by Elsevier Ltd on behalf of Institution of Chemical Engineers. This is an open access article under the CC BY-NC-ND license (<http://creativecommons.org/licenses/by-nc-nd/4.0/>).

considered one of the most troublesome wastes as it is difficult to treat in an environmentally benign manner (Kim, 2001) which can be attributed to the high chlorine content in PVC. Upon thermal treatment, large amounts of hydrogen chloride (HCl) are evolved along with undesirable chlorinated hydrocarbons (dioxins) (Miranda et al., 1999). Due to these issues, the most prevalent route for the disposal of PVC is landfilling. However, the study conducted by (Mersiowsky et al., 1999) suggests a high stability of PVC in landfills. Hence, landfilling results in the indefinite accumulation of PVC which will lead to the occupation of vast dumping areas. Therefore, it is suggested that the most suitable way for recycling PVC would be pyrolysis with mitigation of the emissions accompanied by the thermal decomposition using additives such as metal oxides.

Recent research has focused on the co-thermal treatment of PVC with metallurgical wastes such as EAFD and with metal oxides (Al-Harrahshah, 2017; Al-Harrahshah et al., 2021a, 2021b; Altarawneh et al., 2021; Ji et al., 2020; Lee and Song, 2007; Meng et al., 2021; Ye et al., 2021). The reason behind these studies is to show the capability of metal oxides for mitigating the harmful emissions evolved from decomposing PVC, which would allow recycling via pyrolysis/incineration. (Lee and Song, 2007) confirmed the formation of zinc, lead, and cadmium chlorides upon the thermal treatment of EAFD with PVC. A series of papers published by Al-Harrahshah et al. studied the kinetics (Al-Harrahshah et al., 2015), thermodynamics (Al-Harrahshah, 2017), and zinc and lead extraction possibility (Al-Harrahshah et al., 2022, 2021a, 2021b; Al-harrahshah et al., 2014) upon the co-thermal treatment of EAFD with PVC. However, none of these papers identified the specific effect of each EAFD constituent on the kinetics of the decomposing PVC. Such an aspect is important since the chemistry of EAFD varies greatly from one country to another making it difficult to extrapolate the results from one specific EAFD from a certain country to all other EAFD generated world-wide. Hence, there has been a focus on establishing a solid foundation on the pyrolysis of PVC with each metal oxide separately. (Ye et al., 2021) studied the effect of magnetite (Fe_3O_4) on the emissions of decomposing PVC and its ability to capture HCl. (Meng et al., 2021) studied the effect of seven metal oxides: CaO, ZnO (two types), CuO, MgO, Al_2O_3 and Fe_2O_3 on the thermal degradation of PVC including the onset and maximum rate temperature and their ability to capture HCl. (Altarawneh et al., 2021) studied the effect of ZnO on the kinetics of degrading PVC and the capability of ZnO to capture HCl. To the best of our knowledge, the only study addressed the effect of ZnFe_2O_4 on the decomposition of PVC was that conducted by (Zhang et al., 2000). However, that study focused on characterising the gaseous emissions from PVC degradation in the presence of ZnFe_2O_4 without a deep consideration of the kinetics aspect of the decomposition.

Since ZnFe_2O_4 is considered one of the main sources of zinc in EAFD; reported at 20.27 wt% of EAFD (Al-Harrahshah, 2017), we believe that a comprehensive systematic non-isothermal kinetic study of ZnFe_2O_4 -PVC (ZF-PVC) mixture should provide researchers in this field with valuable information regarding reaction rates. This contributes towards process optimisation in terms of optimum operating temperatures, holding times, and reactor sizing to achieve a certain extraction/conversion levels. Herein, an attempt is made to study the thermal behaviour of PVC and its mixture with ZnFe_2O_4 along with a complete characterisation of the solid products generated from their pyrolysis. The kinetic data associated with the thermal degradation of PVC and its mixture with ZnFe_2O_4 were extracted. The kinetic data was then used for the assessment of the chemical stability of PVC and how it reflects on the selective extraction of zinc.

2. Non-isothermal kinetics

2.1. The overall rate equation

The reaction rate of thermally stimulated processes is usually represented by the extent of conversion X , which is given as follows:

$$X = \frac{W_o - W}{W_o - W_f} \quad (1)$$

Where W_o is the initial weight% at the beginning of the mass loss, W_f is the final weight% at the end of the mass loss, and W is the weight% at any time t . The kinetic rate equation can be represented by the temperature dependent rate constant $k(T)$ and the temperature independent reaction model $f(X)$ (Al-Harrahshah et al., 2018):

$$\frac{dX}{dt} = k(T)f(X) \quad (2)$$

The temperature dependency of the reaction rate can be represented through the Arrhenius function (Vyazovkin et al., 2011):

$$k(T) = A.exp\left(-\frac{E}{RT}\right) \quad (3)$$

Where A is the frequency factor (min^{-1}), E is the activation energy (J/mol), R is the universal gas constant (8.314 J/mol.K), and T is the temperature (K).

The mathematical formula for the reaction model $f(X)$ depends on the controlling mechanism of the overall mass loss. A generalised empirical model was introduced by (Sesták and Berggren, 1971) for the mathematical expression of $f(X)$ as follows:

$$f(X) = X^m(1-X)^n[-\ln(1-X)]^p \quad (4)$$

A different combination of m , n , and p resemble different reaction models (Vyazovkin et al., 2011). Substituting Eqs. (3 and 4) in 2 yields the following:

$$\frac{dX}{dt} = A.exp\left(-\frac{E}{RT}\right)(X^m(1-X)^n[-\ln(1-X)]^p) \quad (5)$$

Eq. (5) represents the rate equation in the differential form. For non-isothermal kinetics at a fixed heating rate of $\beta = \frac{dT}{dt}$, the differentiation of the conversion X can be represented with respect to temperature T as follows:

$$\frac{dX}{dt} = \frac{dT}{dt} \frac{dX}{dT} = \beta \cdot \frac{dX}{dT} \quad (6)$$

Substituting Eq. (6) in 5 yields:

$$\beta \cdot \frac{dX}{dT} = A.exp\left(-\frac{E}{RT}\right)(X^m(1-X)^n[-\ln(1-X)]^p) \quad (7)$$

Re-arranging Eq. (7) and integrating both sides generates the integral form of the rate equation, which can be written as:

$$\int_0^X \frac{dX}{(X^m(1-X)^n[-\ln(1-X)]^p)} = \frac{A}{\beta} \int_{T_o}^T exp\left(-\frac{E}{RT}\right) dT \quad (8)$$

Where T_o is the temperature corresponding to a conversion of zero. At low temperatures, the reaction rate is very low (Ozawa, 1965) making the replacement of T_o by zero a valid assumption:

$$\int_0^X \frac{dX}{(X^m(1-X)^n[-\ln(1-X)]^p)} = \frac{A}{\beta} \int_0^T exp\left(-\frac{E}{RT}\right) dT \quad (9)$$

The right hand side of Eq. (9) has no exact integration (Coats and Redfern, 1964). Hence, different approaches were followed to either utilise the differential form of the rate equation (Eqs. 5 or 7) or the integral form (Eq. 9) whereby the temperature integration is approximated.

2.2. Calculation of the activation energy

2.2.1. Iso-conversional kinetic methods

The iso-conversional principle gained its strength from the fact that the activation energy can be obtained without assuming a reaction model. This, in turn, allows the change in the activation energy with conversion for complicated multi-stage decompositions to be tracked. The iso-conversional principle suggests that the reaction rate is a function of temperature only at a fixed conversion value which can be visualised by taking the logarithmic derivative of the rate with respect to the reciprocal of temperature (Vyazovkin et al., 2011):

$$\left[\frac{\partial \ln \left(\frac{dX}{dt} \right)}{\partial T^{-1}} \right]_X = \left[\frac{\partial \ln f(X)}{\partial T^{-1}} \right]_X + \left[\frac{\partial \ln(k(T))}{\partial T^{-1}} \right]_X = \frac{-E_x}{R} \quad (10)$$

Eq. (11) suggests that the change in the rate depends on temperature only at a fixed value of conversion. Thus, when the mass loss curve shows a lateral shift towards a higher temperature at a higher heating rate, this phenomenon can be exploited for extracting the activation energy without needing to assume a reaction model.

2.2.1.1. Integral iso-conversional method. The Kissinger-Akahira-Sunose (KAS) integral equation (Akahira and Sunose, 1971; Kissinger, 1957) can be written as follows:

$$\ln \left(\frac{\beta_i}{T_{x,i}^2} \right) = \ln \left(\frac{A_x R}{E_x g(X)} \right) - \frac{E_x}{RT_{x,i}} \quad (11)$$

This method should ideally be used in cases where the change in the activation energy with conversion is small. A plot of $\ln \left(\frac{\beta_i}{T_{x,i}^2} \right)$ against $\frac{1}{T_{x,i}}$ should produce a straight line with a slope of $-\frac{E_x}{R}$ from which the activation energy is extracted.

2.2.1.2. Differential iso-conversional method. By taking the natural logarithm on both sides of Eq. (7), one arrives at the Friedman model (Friedman, 1964):

$$\ln \left[\beta_i \frac{dX}{dT} \right]_{X,i} = \ln \left[\frac{dX}{dt} \right]_{X,i} = \ln[A_x f(X)]_{X,i} - \frac{E_x}{RT_{x,i}} \quad (12)$$

For a mass loss with a smooth (non-noisy) derivative thermogravimetric (DTG) signal, the Friedman method can be used to extract activation energies at a higher accuracy compared to the KAS method. This is because unlike the KAS method, the Friedman method does not use any approximation, but instead, it uses the rate equation in its raw form, and hence yielding the most accurate kinetic data. Plotting $\ln \left[\beta_i \frac{dX}{dT} \right]_{X,i}$ against $\frac{1}{T_{x,i}}$ must yield a straight line with a slope of $-\frac{E_x}{R}$ from which the activation energy is obtained.

2.3. Calculation of the frequency factor

2.3.1. The compensation effect

Calculation of the frequency factor with high accuracy can be achieved using the compensation effect (Vyazovkin, 2021). This method relies on the principle that the values of $\ln(A)$ and E are linearly related regardless of being correct or not (Vyazovkin, 2021). The linear dependency maybe presented as:

$$\ln(A)_i = aE_i + b \quad (13)$$

Such that a and b are constants. A set of values of $\ln(A)$ and E can be produced by fitting the experimental rate against the reciprocal of temperature using different sets of $f(X)$ as shown in Eq. (15). The experimental rate can be estimated by differentiating Eq. (1) with respect to time which yields Eq. (14):

$$\frac{dX}{dt} = \frac{-1}{W_o - W_f} \frac{dW}{dt} \quad (14)$$

Such that $\frac{dW}{dt}$ is the value of the experimental DTG signal obtained from the Thermogravimetric analysis. The kinetic models used for generating the compensation data are presented in Table 1.

Once a set of $\ln(A)$ and E are obtained, a plot is constructed, and the data is fitted with a straight line. The resulting linear equation should have the form presented in Eq. (13) from which the values of a and b are obtained. The extracted activation energies using the KAS and the Friedman methods are then inserted into Eq. (13) to obtain conversion dependent frequency factor values $\ln(A)_X$. Further illustration on the compensation effect is presented in detail elsewhere (Vyazovkin, 2021).

2.4. Prediction of the kinetic model

The rearrangement of the differential form of the rate equation (Eq. 7) into the form shown in Eq. (15) allows for the prediction of the controlling reaction model in the studied conversion range by constructing a plot of $\ln \left[\frac{dX}{f(X)} \right]$ against $\frac{1}{T}$. Only the correct mathematical expression of $f(X)$ yields a straight line. The criteria followed for this approach is that the chosen reaction model is the one which yields a straight line and an activation energy as close as possible to that produced from the Friedman model on the studied conversion range.

$$\ln \left[\frac{dX}{f(X)} \right] = \ln(A) - \frac{E}{RT} \quad (15)$$

3. Materials and method

3.1. Thermogravimetric and differential scanning calorimetry analysis

ZnFe₂O₄ used in this work was obtained from Alfa Aesar with a purity of 99% <, while powdered pure PVC was obtained from Sigma-Aldrich. A stoichiometric mixture of ZnFe₂O₄ and PVC (ZF-PVC) was prepared in which the amount of PVC added to ZnFe₂O₄ would be enough to chlorinate it completely to ZnCl₂ and FeCl₃; the calculation was based on the theoretical content of HCl in the PVC monomer. This yielded a mixture containing 32.5 wt% ZnFe₂O₄. The two powders were tumbled in a glass vial containing stainless steel balls for 15 min. The homogeneity of the mixture was confirmed using scanning electron microscopy (SEM) technique and is shown in Fig. S1 (supplementary material).

The instrument used for the thermal analysis was the simultaneous TGA/DSC analyser (TA SDT Q600) which is capable of generating simultaneous mass loss and heat flow signals. Prior to the thermal analysis, an empty ceramic crucible was loaded to generate a base line

Table 1

Kinetic models in the differential $f(X)$ and the integral $g(X)$ form (Georgieva et al., 2013) used to generate the $\ln(A)$ and E data for the compensation effect.

No.	Kinetic model	$f(X)$	$g(X)$
Chemical process			
1	One-third order	$\frac{3}{2}(1-X)^{\frac{1}{3}}$	$1 - (1-X)^{\frac{2}{3}}$
2	Three-quarters order	$4(1-X)^{\frac{3}{4}}$	$1 - (1-X)^{\frac{1}{4}}$
3	One and half order	$2(1-X)^{\frac{3}{2}}$	$(1-X)^{\frac{-1}{2}} - 1$
4	Second order	$(1-X)^2$	$(1-X)^{-1} - 1$
5	Third order	$\frac{1}{2}(1-X)^3$	$(1-X)^{-2} - 1$
6	n^{th} order, $n > 1$	$\frac{1}{n-1}(1-X)^n$	$(1-X)^{-n+1} - 1$

for the heat flow signal. A mass of 9.9 ± 0.07 and 10.2 ± 0.30 mg of PVC and ZF-PVC mixture, respectively were then loaded in a ceramic crucible and the thermal analysis was performed in the temperature window 25–900 °C under a nitrogen flow of 100 mL/min. Using a small sample mass can help in reducing the thermal gradient between the furnace and the sample for more reliable data. The repeatability of the thermogravimetric scan for the de-hydrochlorination stage has been tested on the degradation of ZF-PVC mixture at a heating rate of 10 °C/min (Fig. S8). Three heating rates of 10, 30, and 50 °C/min were used during the analysis which are essential for the model-free (iso-conversional) kinetic calculations.

3.2. Particle size analysis

The contact surface area can have a significant impact on the reaction efficiency between solid reactants. The particle sizes for both ZnFe_2O_4 and PVC were analysed using Beckman Coulter LS13320MW laser diffraction analyser with an Aqueous Liquid Module (ALM). The particle sizes for both ZnFe_2O_4 and PVC are presented in Table 2.

3.3. Pyrolysis of ZF-PVC mixture

A sample of 0.31 ± 0.0001 g of the ZF-PVC mixture was loaded into a 4 mm quartz tube on top of a porous ceramic fibre disk. The ceramic fibre disk acts as a sample holder and helps in distributing the gas flowing through the sample. Another ceramic fibre disk was loaded on top to prevent the powder from fluidising. The tube with the powder was purged with N_2 (99.9992% pure) for at least 15 min before starting the heating. This ensured that the reactants were completely surrounded by a nitrogen blanket. Three pyrolysis temperatures were studied: 260, 420, and 650 °C. The choice of these temperatures was based on the plateau temperature after each stage on the TGA scans. The furnace was heated to the desired temperature, the reactants were then inserted and held at that temperature for 30 min. The products generated from the pyrolysis were isolated as fast as possible and transferred to a glass vial. The glass vial was then purged with nitrogen and stored in a desiccator for further analysis.

3.4. Mineralogy of the pyrolysis residue

The mineralogy of the pyrolysis residues was studied using the X-Ray diffraction (XRD) technique. Due to the hygroscopic nature of the powders, each pyrolysis residue was analysed individually (i.e., they were not loaded into the XRD instrument at the same time). Moreover, the powder on the sample holder was covered with a piece of tape to prevent air from being in contact with the powder which can potentially alter the mineralogical phase. The X-Ray tube on the Bruker D8 Advance XRD instrument was operated at a current and voltage of 40 mA and 40 kV, respectively and the analysis was performed in the 2 θ range 5–90°, step size of 0.02° with a scanning time of 1.7 s/step. Qualitative interpretation of the XRD patterns was performed using DIFFRAC.EVA V5.2 software which utilises the PDF-2 database.

3.5. Morphology and chemistry of the pyrolysis residue

The morphology and the chemistry of the pyrolysis residue were studied using scanning electron microscopy (SEM) coupled with energy

dispersive spectroscopy (EDS) techniques. Powders generated from the pyrolysis were sprinkled on a stub covered with an adhesive carbon layer. Due to the poor electrical conductivity of the powders, they were coated with a conductive layer of carbon with a thickness of 6 nm. Stubs with the powder on them were then inserted into an FEI Quanta600 MLA SEM instrument where an electron beam with a spot size of 5.0 and an accelerating voltage of 15.0 kV were used for the analysis. The choice of these parameters generated an electron beam with a sufficient energy to perform EDS analysis which allowed studying the chemistry of the generated crystals.

3.6. Thermodynamic simulation

The equilibrium amounts of the expected species during the pyrolysis in the temperature range 200–1000 °C were studied using FACT-SAGE 7.3 software. FACT-SAGE software implements the Gibbs free energy minimisation method (Bale et al., 2016, 2002) to calculate the amounts of chemical species when the specified compounds react partially or totally to achieve a state of chemical equilibrium. The chlorine in PVC was added in the simulation as gaseous HCl such that its molar amount was calculated from its stoichiometry in the PVC monomer. The carbon added to the system was based on the final char amount in the crucible after the TGA experiments, while H_2 was assumed to constitute half of the 6.7% excess mass loss from the de-hydrochlorination stage (6.7% over the theoretical HCl content). The molar amounts of ZnFe_2O_4 , HCl, H_2 , and C were added based on their respective amounts in the mixture prepared experimentally which gave the following molar values: 13.48, 107.9, 115.3, and 34.3 mol, respectively. The simulation was carried out in two stages: the first stage extending from 200 to 430 °C which represents the de-hydrochlorination stage while the latter extends from 430 to 1000 °C representing the polyene thermal cracking stage. In the second stage, N_2 gas was introduced to the system with an amount of 69.91 mol which serves as a medium for mass transfer (volatilisation of formed chlorides). This amount was based on the amount of gaseous emissions in the second stage (which were inert) and hence was substituted as N_2 to act as a medium for mass transfer. Products from the first stage were added to the second stage except for gaseous ones which were assumed to escape from the reaction system.

The purpose of these calculations is to support the experimental observations obtained in the pyrolysis residues and to help predicting certain chemical and physical processes (reactions, volatilisation, etc.). This, in turn, makes the interpretation of the kinetic data easier since the dominant chemical species and reactions are known versus temperature.

4. Results and discussion

4.1. Thermodynamic speciation of ZF-PVC pyrolysis

The equilibrium amounts from the pyrolysis of ZF-PVC mixture are presented in Fig. 1(a) and (b). From a temperature of 200 °C both ZnCl_2 and FeCl_2 appear in their solid form with a complete absence of ZnFe_2O_4 , ZnO , and Fe_2O_3 (Fig. 1(a)). This suggests that ZnFe_2O_4 was completely chlorinated yielding ZnCl_2 , Fe_2O_3 and $\text{H}_2\text{O}_{(g)}$. Fe_2O_3 is then immediately reduced by H_2 to Fe^{2+} bearing oxide (Fe_3O_4) which is then chlorinated into FeCl_2 . Solid ZnCl_2 then starts transforming into the liquid form at a temperature of 310 °C which subsequently starts evaporating to the gaseous form at a temperature of 430 °C and becomes almost entirely present in the gaseous form at a temperature of 630 °C (Fig. 1(b)). Liquid FeCl_2 , in contrast, starts appearing at a temperature of 680 °C and immediately starts volatilising above that temperature until it is entirely present in the gaseous form at a temperature of 880 °C. The carbon in Fig. 1(b) remains inert over the entire temperature range in the absence of any zinc or iron oxide species.

Overall, the thermodynamic data suggests that ZnFe_2O_4 , a major zinc source in EAFD, should be completely removed and transformed into chloride forms of zinc and iron upon thermal treatment with a

Table 2
The mean particle sizes of PVC and ZnFe_2O_4 measured using the laser diffraction technique.

Material	Mean particle size, μm^a
PVC	158.8 ± 18.5
ZnFe_2O_4	13.2 ± 4.2

^a : Mean \pm SD

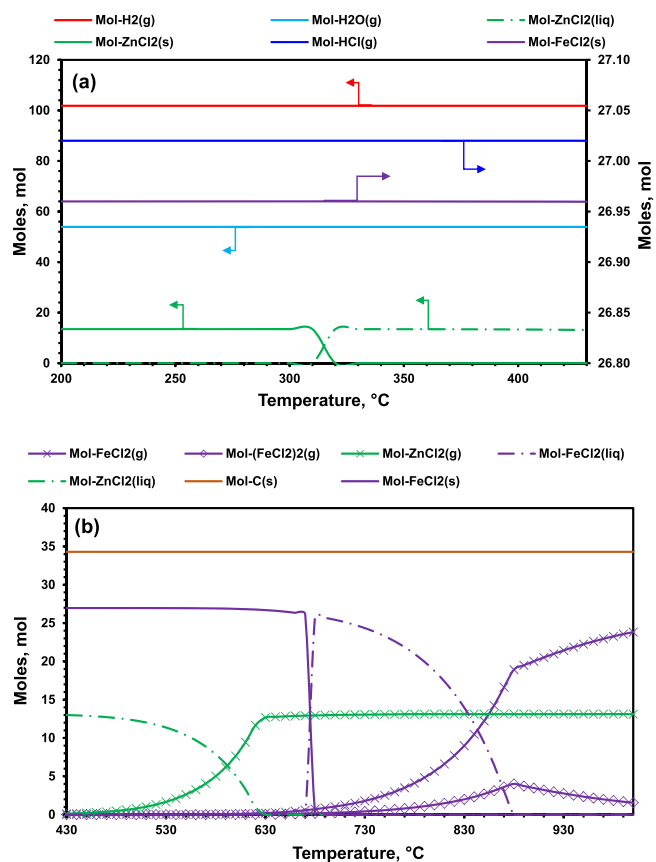


Fig. 1. Thermodynamic simulation of the reactants/products from the pyrolysis of the ZF-PVC mixture (32.5 wt% ZnFe_2O_4) in the temperature window 200 – 430 °C (a) and 430 – 1000 °C (b).

stoichiometric quantity of PVC. The kinetic barriers contributing towards selective zinc chlorination will be shown in later sections.

4.2. Experimental thermal behaviour of PVC and ZF-PVC mixture

The thermal degradation profiles of pure PVC and ZF-PVC mixture at different heating rates are presented in Fig. 2(a) and (b). The decomposition of pure PVC occurs in three stages, while that of ZF-PVC follows four stages. The first two overlapped stages for pure PVC start at a temperature of 272 °C and produce a mass loss of about 65%. These stages involve the de-hydrochlorination of PVC through the evolution of HCl along with volatiles (Jordan et al., 2001) and the evolution of small amounts of H_2 (Ye et al., 2021). The de-hydrochlorination of PVC absorbs a large amount of energy which is evident from the large endothermic peak extending from 250 to 320 °C (Fig. 3). The occurrence of the de-hydrochlorination in the form of a two overlapped stages for pure PVC is discussed in more detail in the kinetics Section 4.3. At the end of these stages, most of the chlorine in the PVC was stripped out of the polymer chain (Yu et al., 2016) and the remaining solid was reported to be a conjugated polyene structure (Marcilla and Beltrán, 1995).

When a stoichiometric quantity of ZnFe_2O_4 was added to PVC, the onset de-hydrochlorination temperature of PVC dropped appreciably to a value of 235 °C suggesting a catalytic effect of ZnFe_2O_4 on PVC degradation. A similar effect was reported before by (Altarawneh et al., 2021) for ZnO such that the addition of a stoichiometric quantity of ZnO resulted in an even larger drop in the de-hydrochlorination onset temperature to a value of 214 °C (compared to 272 °C for pure PVC). Such behaviour for both ZnO and ZnFe_2O_4 can be attributed to the direct reaction of these oxides with the chlorine atom in the PVC monomer forming metallic chlorides/oxychlorides while simultaneously

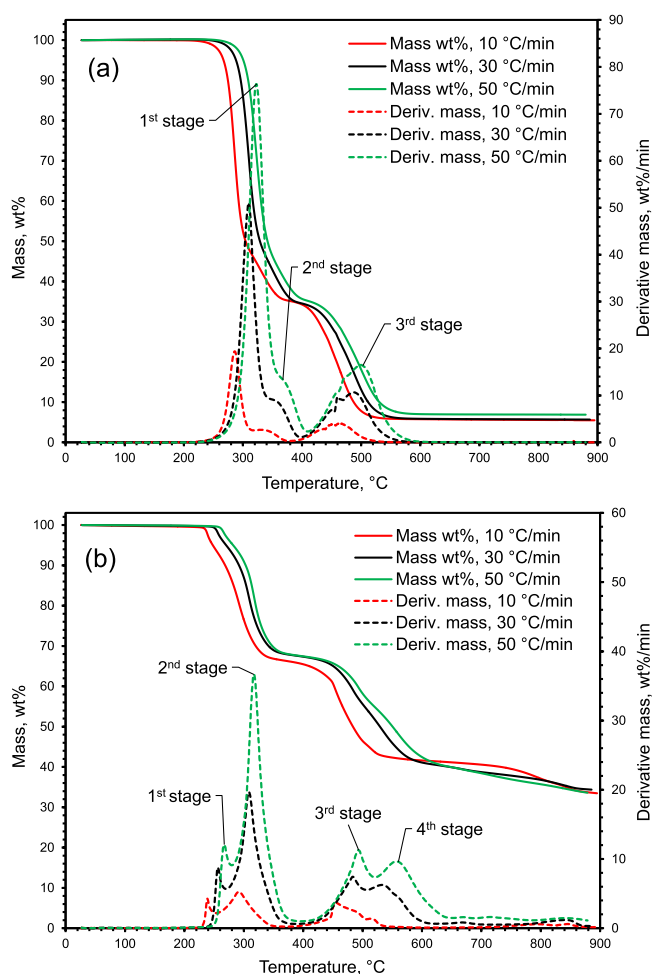


Fig. 2. Thermal degradation of pure PVC (Altarawneh et al., 2021) (a) and ZF-PVC (32.5 wt% ZnFe_2O_4) mixture (b) at heating rates of 10, 30 and 50 °C/min and under a nitrogen flow of 100 mL/min.

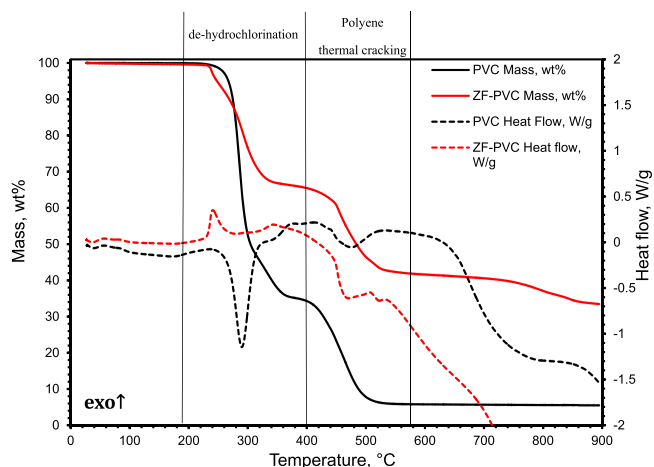
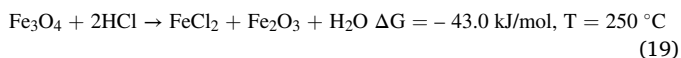
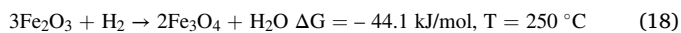
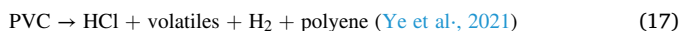
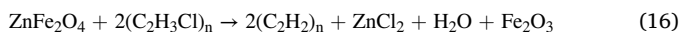


Fig. 3. TGA/DSC profiles of pure PVC and ZF-PVC (32.5 wt% ZnFe_2O_4) under a nitrogen flow of 100 mL/min and a heating rate of 10 °C/min.

generating gaseous H_2O . The mass spectrometric data reported by (Zhang et al., 2000) of the emissions generated from ZF-PVC mixture is also in line with the results presented here. In their work, H_2O mass peaks were detected which can be assigned to the chlorination of ZnFe_2O_4 by PVC. These chlorination reactions can be written according

to the following sequence:



Evidence for the chlorination reaction can be seen from the exothermic peak associated with the ZF-PVC mixture (absent for pure PVC) as shown in Fig. 3. Additionally, this exothermic peak starts appearing at 227 °C which is much lower than the de-hydrochlorination onset temperature of pure PVC suggesting a direct reaction of ZnFe₂O₄ with PVC. Likewise, the addition of ZnFe₂O₄ also changed the DTG signal drastically into a doublet peak that the first peak is associated with the direct reaction of ZnFe₂O₄ with PVC (H₂O evolution) while the second one is attributed to the normal de-hydrochlorination of PVC (HCl evolution) along with H₂O evolved from the reduction of Fe₂O₃ by H₂ and its consecutive chlorination.

The occurrence of Reactions 16, 18 and 19 is confirmed from the XRD patterns presented in Fig. 4 which are related to the pyrolysis residues of ZF-PVC at temperatures of 260, 420, and 650 °C. At a temperature as low as 260 °C, ZnFe₂O₄, which is known for its chemical stability (Havlik et al., 2006), was completely destroyed, and transformed into Lawrencite (FeCl₂), Rokuhnite (FeCl₂·2H₂O), and Hematite (Fe₂O₃). This result is in agreement with the thermodynamic data presented earlier. The presence of Fe₂O₃ here and its absence in the thermodynamics section might be assigned to kinetics whereby the reduction of Fe₂O₃ by H₂ was not fast enough to make it completely disappear at 260 °C. This result is in agreement with the work done by (Pineau et al., 2006) where at a temperature of 258 °C the reduction of Fe₂O₃ by H₂ was very slow needing up to 500 min to reach a conversion of ~88%. The slow reduction kinetics at low temperatures is also confirmed from the XRD data shown in Fig. 4 where Fe₂O₃ is completely reduced and chlorinated only at a higher temperature of 420 °C. Despite the complete disappearance of ZnFe₂O₄ in the 260 °C pattern, no ZnCl₂ peaks could be detected. In a previous study conducted by (Altarawneh et al., 2021) for the co-pyrolysis of ZnO with PVC, peaks of α-ZnCl₂, ZnCl₂·1.33H₂O and Zn(OH)Cl/ZnOCl₂·2H₂O were detected, however, with small intensities. ZnCl₂ is also known to be a deliquescent material which tends to dissolve itself in in-situ solution when a sufficient amount of water is absorbed to the surface. In fact, (Altarawneh et al., 2021) reported that ZnCl₂ completely disappeared and recrystallised in the form of Simonkolleite (Zn₅(OH)₈Cl₂·H₂O) when exposed to the

atmosphere for long period of times (~ 6 h). This means that at some point, ZnCl₂ dissolves into an aqueous solution which upon saturation, recrystallises as Zn₅(OH)₈Cl₂·H₂O. Such behaviour makes the detection of crystalline ZnCl₂ very difficult to achieve.

The formation of ZnCl₂, however, can be confirmed from the SEM analysis at a temperature of 650 °C (Fig. 5). According to the thermodynamic simulation presented earlier, at a temperature of 650 °C, ZnCl₂ can only be present in its gaseous form. Such behaviour explains the absence of zinc upon EDS scanning of a large surface area of the pyrolysis residue at 650 °C for two minutes (Fig. 5). The spectra presented under the maps in Fig. 5 also shows that zinc has almost zero counts per second suggesting a complete chlorination of ZnFe₂O₄ followed by the evaporation of formed ZnCl₂. In Fig. S7 in the supplementary material, it is shown that ZnFe₂O₄ remains stable up to 900 °C. Hence, the only way zinc would disappear from the SEM/EDS images, is that ZnFe₂O₄ was completely chlorinated and formed ZnCl₂ was then volatilised. This result is in a good agreement with the thermodynamics section presented above.

At 260 °C, incomplete chlorination of iron takes place which is evident from the Fe₂O₃ peaks appearing in Fig. 4 (pattern (b)). When the pyrolysis temperature is increased to 420 °C, all Fe₂O₃ peaks disappear giving rise to FeCl₂ and FeCl₂·2H₂O peaks with higher intensities. Contrary to zinc, the maps in Fig. 5 show the presence of iron which is associated with chlorine. Such a result is in line with the XRD pattern (d) in Fig. 4 with peaks of both FeCl₂ and FeCl₂·2H₂O. This result also agrees with the thermodynamics data presented earlier.

The effect of temperature on the degree of chlorination of iron bearing compounds is important for the optimisation and the proper selection of temperature to yield high zinc extraction while simultaneously leaving iron in non-leachable form (oxide form). Further illustration on this is presented in the kinetics Section 4.3.

The third decomposition stage for pure PVC extending from 400 to 520 °C is associated with the thermal cracking of polyene formed from the de-hydrochlorinated PVC into volatiles such as polyenyl aromatics, alkyl aromatics, and polyaromatics (Blazso and Jakab, 1999). About 6% of the initial weight of the sample was left in the crucible which is characterised as char. The formation of char is confirmed from its oxidation when PVC is heated under air showing a large exothermic peak and a drop of the wt% to zero (Fig. S2). Under pyrolytic conditions, however, the cracking of polyene is endothermic as shown in Fig. 3.

For a ZF-PVC mixture, the polyene thermal cracking stage extending from 400 to 540 °C appears as a doublet. This is attributed to the simultaneous polyene thermal cracking and the volatilisation of formed ZnCl₂. This is also evident from the heat flow signals appearing in Fig. 3 for ZF-PVC showing endothermic doublet which is absent in the case of pure PVC. The evaporation of ZnCl₂ in that stage has a large kinetic effect which will be discussed in the next section.

4.3. Non-isothermal kinetics of PVC and ZF-PVC degradation

4.3.1. Kinetics of the de-hydrochlorination stage

In this section, the kinetic parameters associated with the de-hydrochlorination stage resembled by the first two stages for both pure PVC and ZF-PVC mixture (Fig. 2(a) and (b)) are presented. Fig. 6 shows a comparison of the activation energy associated with the de-hydrochlorination of pure PVC and ZF-PVC mixture at different conversion levels. The activation energy for pure PVC de-hydrochlorination starts at 109.9 kJ/mol at a conversion of 0.004 and remains almost constant up to a conversion of 0.7 after which an increase to an average value of 167.1 kJ/mol occurs at conversions of 0.8–0.9. Such behaviour indicates that two mechanisms control the degradation of pure PVC as presented in Table 3 where two different reaction models ($f(X)$) could fit different conversion ranges. Initially, the truncated Šesták and Berggren function $f(X) = X(1 - X)^{2.13}$ fits the experimental data in the conversion range 0.1 – 0.6 (all experimental data fitting are presented in the

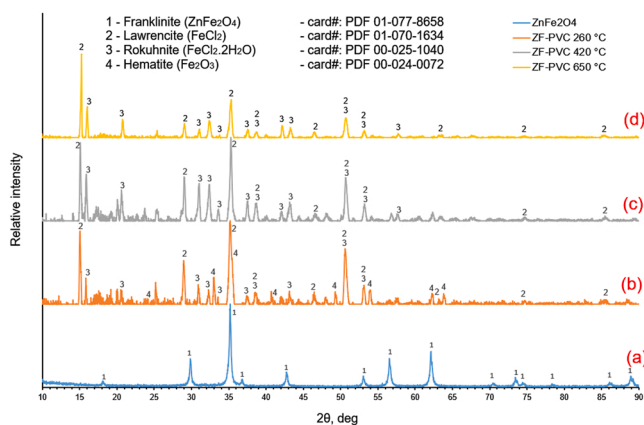


Fig. 4. XRD patterns of the pyrolysis residues of ZF-PVC (32.5 wt% ZnFe₂O₄) mixture under an inert (nitrogen) environment for 30 min at different temperatures of (a) room temperature (ZnFe₂O₄ alone), (b) 260, (c) 420, and (d) 650 °C.

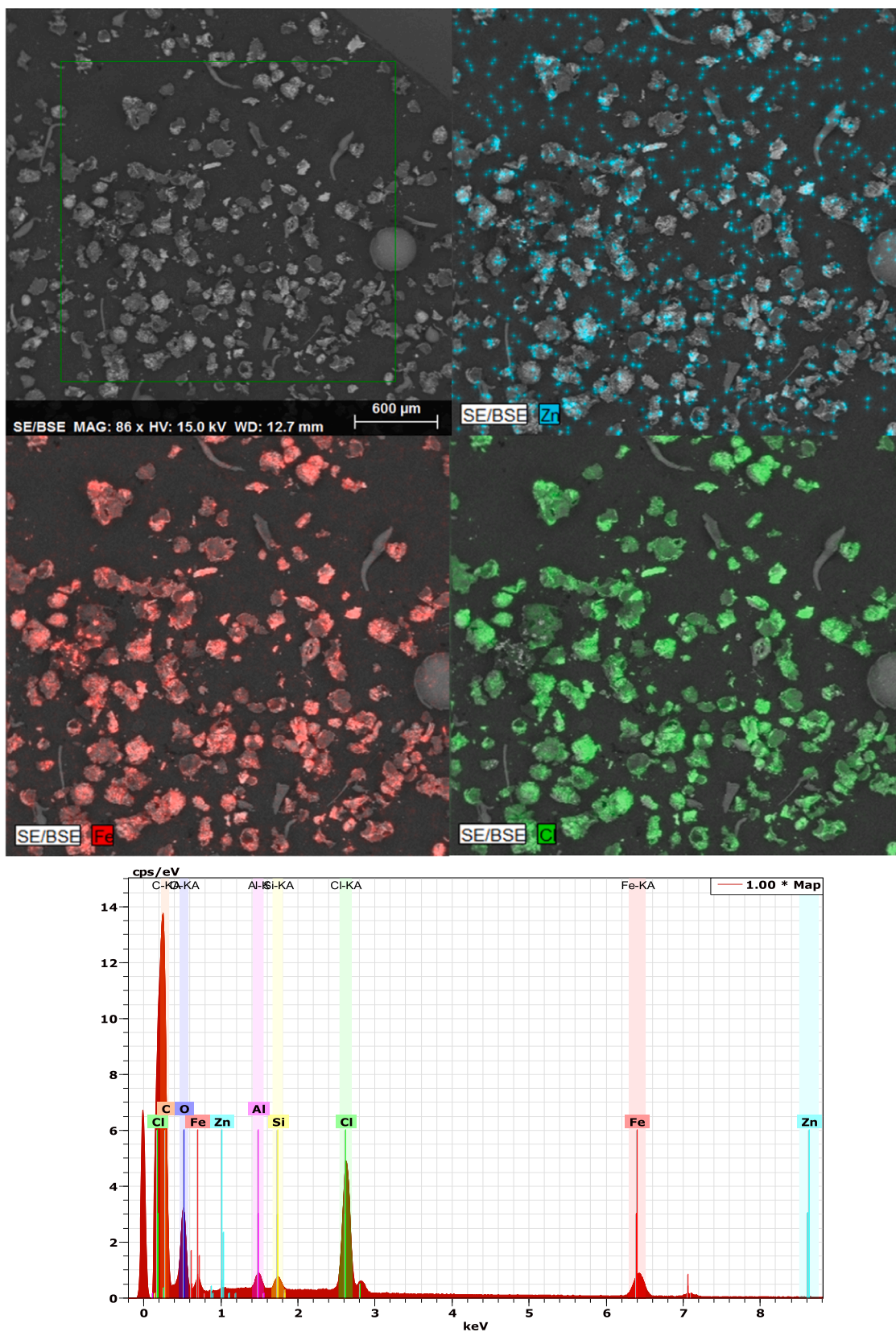


Fig. 5. SEM/EDS scans of the pyrolysis residue of ZF-PVC (32.5 wt% ZnFe₂O₄) at a temperature of 650 °C under an inert (nitrogen) environment for 30 min.

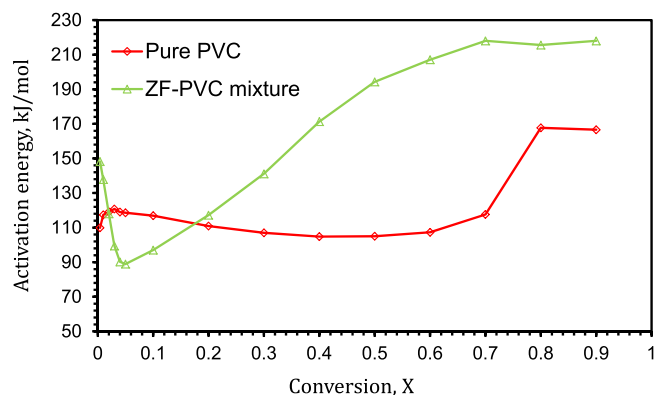


Fig. 6. Iso-conversional activation energies associated with the de-hydrochlorination (first and second stages for both pure PVC and ZF-PVC) in the conversion range 0.004 – 0.9 using Friedman model.

supplementary material Section 3). This type of function is considered an example of an auto catalytic model (Vyazovkin et al., 2011). This agrees with the work done by (Starnes and Ge, 2004) where it was confirmed that the de-hydrochlorination of PVC is auto catalysed by the emitted HCl from PVC decomposition. At a conversion above 0.7, the decomposition becomes controlled by a different reaction model $f(X) = (1 - X)^2$ which is also accompanied by an increase in the activation

energy. This could be assigned to the lean amount of HCl present at the end of the de-hydrochlorination which ceases its catalytic effect. Overall, there is a great degree of agreement between the average activation energy calculated in this work for the pure PVC de-hydrochlorination at 122.6 kJ/mol compared to that calculated and reported in the ICTAC kinetic committee recommendations (Vyazovkin et al., 2020) at 128.5 kJ/mol (both calculated using Friedman model). This confirms the validity of the followed procedure for calculating the kinetic data.

The addition of a stoichiometric quantity of $ZnFe_2O_4$ to PVC resulted in a drastic variation in the activation energy of de-hydrochlorination with conversion. The activation energy at $X = 0.004$ increased from 109.9 to 148.2 kJ/mol (Fig. 6). This result means that the initiation mechanism for the de-hydrochlorination of PVC significantly changes in the presence of $ZnFe_2O_4$, such that for pure PVC, the de-hydrochlorination proceeds via the well-known zipper elimination mechanism (Levchik and Weil, 2005) by which small amounts of HCl initially evolves followed by the formation of labile allylic chlorine sites from which the decomposition proceeds at a fast rate. When $ZnFe_2O_4$ is added, it abstracts chlorine directly from the PVC monomer forming $ZnCl_2$ and Fe_2O_3 , hence the change in the activation energy.

The catalytic activity of $ZnFe_2O_4$ can be shown in the schematic illustration presented in Fig. 7 where the rate constant was calculated at the same temperature of 230 °C (503 K) for both mechanisms A and B. The addition of $ZnFe_2O_4$ accelerated the de-hydrochlorination despite the increase in the activation energy (Fig. 7). It can be seen that the combined activation energy and frequency factor at a temperature of

Table 3

Kinetic parameters associated with the de-hydrochlorination of pure PVC (Fig. 3) (Altarawneh et al., 2021).

Conversion, X	KAS		Friedman			Linear model fitting		
	Activation energy, kJ/mol	Frequency factor, $\ln(A)^a$	Activation energy, kJ/mol	$\ln(A.f(X))$	Frequency factor, $\ln(A)^a$	Activation energy, kJ/mol	Frequency factor, $\ln(A)^a$	f(X)
0.1	118.2	25.03	116.9	23.52	24.74	110.5	24.60	$X(1 - X)^{2.13}$
0.2	116.0	24.53	110.9	22.59	23.37			
0.3	114.3	24.14	107.0	21.88	22.48			
0.4	113.5	23.96	104.8	21.38	21.98			
0.5	112.6	23.76	105.0	21.28	22.03			
0.6	112.1	23.64	107.3	21.41	22.55			
0.7	112.9	23.83	117.6	22.88	24.89			
0.8	125.2	26.62	167.7	31.54	36.28	Transition region (no fitting)		
0.9	153.2	32.99	166.6	29.84	36.03	158.3	32.65	$(1 - X)^2$
Average ^b	119.8 ± 12.4	25.39 ± 2.83	122.6 ± 24.2	24.04 ± 3.65	26.04 ± 5.50	—		

^a : Unit of frequency factor (A) is min^{-1}

^b : Average = mean ± SD

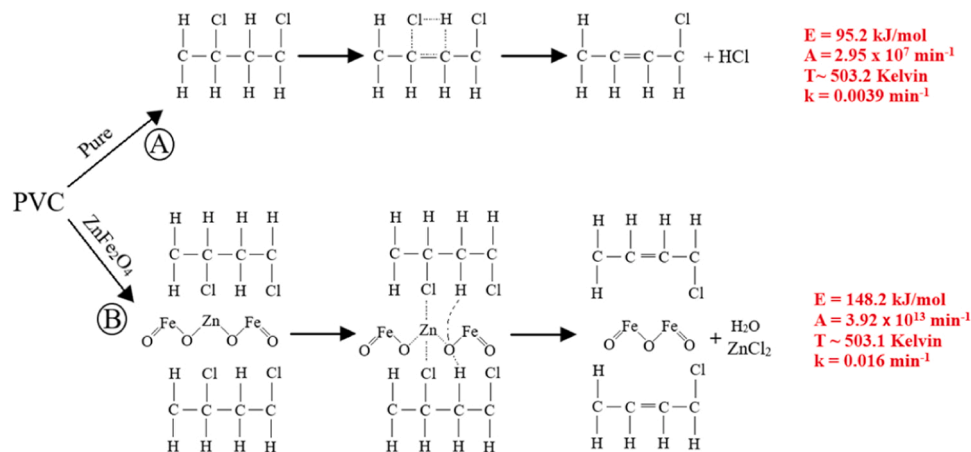


Fig. 7. The de-hydrochlorination of PVC with and without $ZnFe_2O_4$ along with the kinetic parameters associated with the de-hydrochlorination calculated at a temperature of ~ 503 K showing the higher rate constant (k) for ZF-PVC mixture compared to pure PVC; equivalent conversion values for PVC and ZF-PVC at that temperature at a heating rate of 10 °C/min are 0.00044 and 0.004, respectively.

230 °C yielded a rate constant for ZF-PVC mixture (mechanism B) 4.1 times higher than that associated with pure PVC with values of 0.016 and 0.0039 min⁻¹ for ZF-PVC and pure PVC, respectively. Such a result supports what was observed in the thermogravimetric scans where a drop in the onset temperature of the de-hydrochlorination was seen when ZnFe₂O₄ was added to PVC. This also means that reaction channelling towards mechanism B over A can potentially take place when low temperature (e.g., 230 °C) is used in the ZF-PVC mixture.

From conversions extending from 0.03 to 0.1 (Fig. 6) a significant drop in the activation energy to a value as low as 88.9 kJ/mol is seen followed by a continuous increase reaching a maximum of 218 kJ/mol at a conversion of 0.9. The drop in activation energy between conversions 0.03 – 0.1 (corresponds to temperatures 237 – 243 °C) was previously reported by (Altarawneh et al., 2021) for the co-pyrolysis of ZnO with PVC. This drop was assigned to the decomposition of the formed Zn₂OCl₂·2H₂O/Zn(OH)Cl into ZnCl₂, ZnO and H₂O (Altarawneh et al., 2021), which was also reported in a simulation study conducted by (Ahmed et al., 2018).

An increase in the activation energy above a conversion of 0.2 can be assigned to the start of normal PVC de-hydrochlorination, however, this time, in the absence of HCl due to its capturing by Fe₃O₄ formed from the reduction of Fe₂O₃ by H₂. This can be confirmed from the XRD patterns presented in Fig. 4 showing large peaks of FeCl₂/FeCl₂·2H₂O suggesting HCl capturing. Fe₃O₄, in this case, works as a HCl scavenger, preventing HCl from catalysing the de-hydrochlorination which is the reason behind the increase in the activation energy.

According to the evidence in literature (Pineau et al., 2006) on the reduction of Fe₂O₃ by H₂, it is believed that operating at low temperatures (230 – 235 °C) for the ZF-PVC mixture will result in iron being left in its stable form (Fe₂O₃), while simultaneously zinc is being chlorinated into its chloride counterparts. This is because the reduction of Fe₂O₃ by H₂ was found to be kinetically slow at low temperatures (Pineau et al., 2006).

Despite the continuous increase in the activation energy for ZF-PVC, the de-hydrochlorination experimental data for that mixture was fit using a second order reaction model $f(X) = (1 - X)^2$ in the conversion range 0.2 – 0.9 (Table 4). The reliability of the kinetic data associated with the de-hydrochlorination of pure PVC and ZF-PVC mixture can be confirmed by comparing the experimental rates with the rates calculated using the extracted kinetic parameters (Fig. 8). Clearly, a very good agreement between the model generated data and the experimental data can be seen. The comparison was also performed at different heating rates to confirm that the kinetic parameters can be used to predict reaction rates at different temperatures.

4.3.2. Kinetics of the polyene thermal cracking stage

In this section, the kinetic parameters of the polyene thermal

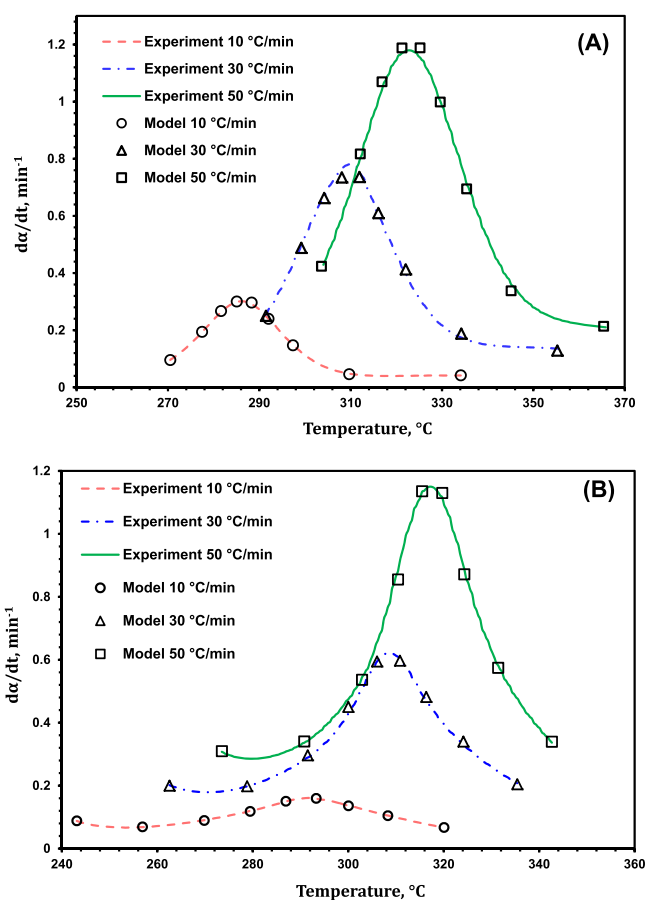


Fig. 8. A comparison between experimental and model generated de-hydrochlorination rates of pure PVC (A) and ZF-PVC mixture (B) at heating rates of 10, 30, and 50 °C/min in the conversion range 0.1 – 0.9 (kinetic data from Friedman model).

cracking stage for pure PVC and ZF-PVC mixture are reported. The activation energy associated with the polyene thermal cracking for both PVC and ZF-PVC is presented in Fig. 9. The activation energy for the polyene thermal cracking is significantly higher than that associated with the de-hydrochlorination of PVC; it starts at 300.6 kJ/mol at a conversion of 0.004 compared with 109.9 kJ/mol for the de-hydrochlorination. Such a result is in agreement with the experimental results where the thermal cracking of the polymer backbone takes place at the significantly higher temperature of 422 °C compared to 272 °C for the de-hydrochlorination. The activation energy then

Table 4

Kinetic parameters associated with the de-hydrochlorination of ZF-PVC mixture (Fig. 3).

Conversion, X	KAS		Friedman			Linear model fitting		
	Activation energy, kJ/mol	Frequency factor, ln(A) ^a	Activation energy, kJ/mol	ln(A.f(X))	Frequency factor, ln(A) ^a	Activation energy, kJ/mol	Frequency factor, ln(A) ^a	f(X)
0.1	115.8	23.63	97.0	20.17	19.16	–	–	–
0.2	109.7	22.18	117.2	23.92	23.96	177.4	37.66	(1 - X) ²
0.3	117.6	24.06	141.1	28.84	29.64			
0.4	130.1	27.03	171.3	35.15	36.83			
0.5	146.5	30.93	194.3	39.83	42.29			
0.6	160.3	34.21	207.1	42.14	45.33			
0.7	178.8	38.60	218.0	43.75	47.92			
0.8	192.2	42.03	215.6	42.34	47.35			
0.9	206.2	45.12	218.0	41.50	47.92			
Average ^b	150.8 ± 33.5	31.98 ± 8.00	175.5 ± 43.89	35.29 ± 8.34	37.82 ± 10.43	—		

^a : Unit of frequency factor (A) is min⁻¹

^b : Average = mean ± SD

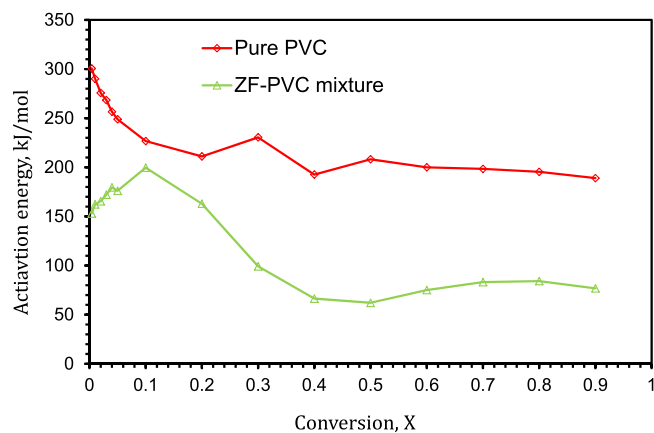


Fig. 9. Iso-conversional activation energies associated with polyene thermal cracking (third stage for pure PVC and third and fourth stages for ZF-PVC) in the conversion range 0.004 – 0.9 using Friedman model.

keeps dropping with conversion averaging at 205.8 ± 13.9 kJ/mol in the conversion range 0.1 – 0.9. The rate of mass loss could be fitted with one reaction model ($f(X) = 2(1 - X)^3$) (Table 5) in the conversion range 0.1 – 0.9 which suggests that the process is chemically controlled over the entire range.

The addition of $ZnFe_2O_4$ to PVC resulted in a drop in the activation energy for the polyene thermal cracking stage. The initiation activation energy at a conversion of 0.004 was 153 kJ/mol compared to 300.6 kJ/mol for pure PVC. This suggests that the presence of different chloride forms ($FeCl_2/FeCl_2 \cdot 2H_2O$ and $ZnCl_2$) can possibly alter the initiation mechanism associated with the cracking of the polymer backbone lowering the activation energy. As the reaction progresses, the activation energy increases to a value of 199.6 kJ/mol at $X = 0.1$ then drops with conversion reaching an average value of 78.1 kJ/mol in the conversion range 0.3 – 0.9. Similar behaviour was previously seen in (Altarawneh et al., 2021) for the polyene thermal cracking of a mixture of ZnO and PVC where the activation energy dropped to an average value of 75.2 kJ/mol between conversions from 0.1 and 0.9. This drop in activation energy is assigned to the volatilisation of $ZnCl_2$ in that temperature range. This is because physical processes (e.g., volatilisation) are known to exhibit lower activation energies compared to chemical ones. Since lumped activation energies are given using Eq. (20) (Vyzovkin et al., 2020) for multi-step processes (parallel processes), the evaporation of $ZnCl_2$ in the same range of the polyene thermal cracking can greatly affect the overall value of the apparent activation energy associated with the mass loss.

Table 5

Kinetic parameters associated with the polyene thermal cracking of pure PVC (Fig. 3) (Altarawneh et al., 2021).

Conversion, α	KAS		Friedman			Linear model fitting		
	Activation energy, kJ/mol	Frequency factor, $\ln(A)^a$	Activation energy, kJ/mol	$\ln(A.f(X))$	Frequency factor, $\ln(A)^a$	Activation energy, kJ/mol	Frequency factor, $\ln(A)^a$	f(X)
0.1	256.2	41.56	226.7	36.66	36.37	201.8	31.67	3
0.2	235.7	37.95	211.1	33.67	33.62			$2(1 - X)^2$
0.3	227.9	36.58	230.5	36.58	37.04			
0.4	219.6	35.12	192.6	30.04	30.36			
0.5	212.5	33.87	208.2	32.24	33.11			
0.6	208.8	33.21	200.0	30.64	31.66			
0.7	205.8	32.69	198.4	30.00	31.38			
0.8	202.4	32.09	195.4	28.99	30.85			
0.9	197.2	31.17	189.0	27.03	29.73			
Average ^b	218.4 ± 17.7	34.92 ± 3.11	205.8 ± 13.9	31.76 ± 3.14	32.68 ± 2.45	—	—	—

^a : Unit of frequency factor (A) is min^{-1}

^b : Average = mean \pm SD

$$E_a = \frac{E_1 k_1(T) f_1(\alpha) + E_2 k_2(T) f_2(\alpha)}{k_1(T) f_1(\alpha) + k_2(T) f_2(\alpha)} \quad (20)$$

Where numbers 1 and 2 in Eq. (20) represent two parallel steps. The thermal cracking for ZF-PVC is controlled by a similar reaction model to that of pure PVC ($f(X) = 2(1 - X)^3$) between conversions 0.1 and 0.2. However, from conversion 0.3 up to 0.8 the mass loss becomes controlled by a first order equation ($f(X) = 1 - X$) (Table 6).

The reliability of the kinetic data for the polyene thermal cracking stage was checked by comparing the experimental rate with the rate generated from the extracted kinetic parameters (Fig. 10). It can be seen that there is a very good agreement between the rate generated from the extracted kinetic data (dotted) and the experimental rate at different heating rates. Making the comparison at different heating rates show that the kinetic data is able to predict the reaction rates at different temperatures.

5. Conclusions

In this work, the thermal behaviour, and the kinetic parameters of PVC degradation alone and in the presence of $ZnFe_2O_4$ have been studied. The de-hydrochlorination of PVC resulted in a complete conversion of $ZnFe_2O_4$ into its chloride species ($ZnCl_2$ and $FeCl_2/FeCl_2 \cdot 2H_2O$). Since $ZnFe_2O_4$ is stable up to 900 °C, the formation of $ZnCl_2$ was confirmed from the disappearance of zinc in the pyrolysis residue at 650 °C suggesting the complete chlorination of $ZnFe_2O_4$ and the evaporation of formed $ZnCl_2$.

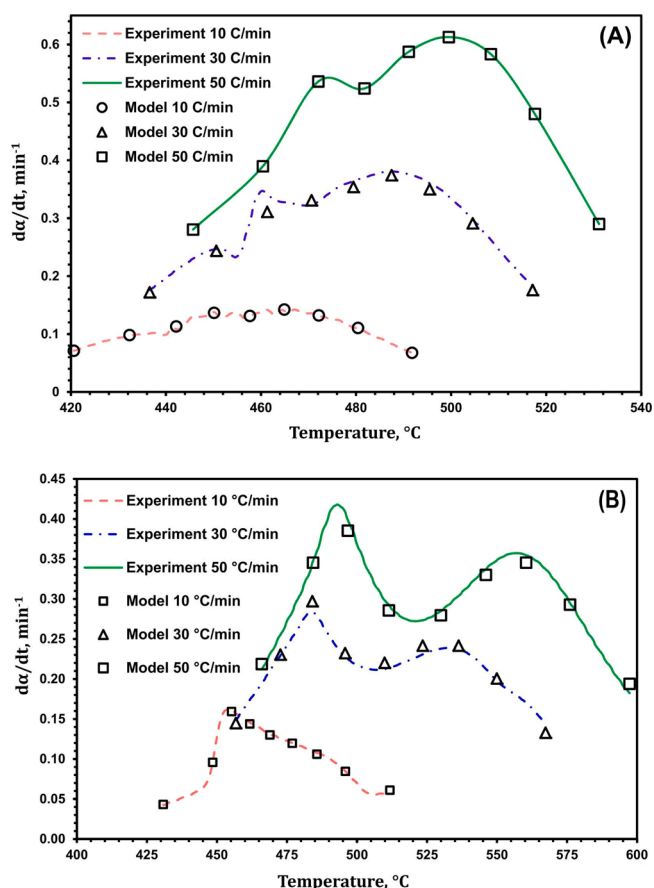
The addition of $ZnFe_2O_4$ catalysed the degradation lowering the de-hydrochlorination onset temperature from 272 °C (pure PVC) to 235 °C (ZF-PVC mixture) despite the increase in the initiation activation energy from 109.9 kJ/mol (pure PVC) to 148.2 kJ/mol (ZF-PVC). This can be assigned to the increase in the frequency factor which compensated for the increase in the activation energy yielding a higher overall rate constant at a lower temperature. The de-hydrochlorination in the presence of $ZnFe_2O_4$ initially proceeds via a direct reaction between $ZnFe_2O_4$ with the PVC monomer eventually yielding $ZnCl_2$ and Fe_2O_3 . Fe_2O_3 is then reduced to Fe_3O_4 by reacting with H_2 from PVC degradation which eventually chlorinates to $FeCl_2$ and $FeCl_2 \cdot 2H_2O$ both of which were detected by XRD.

The kinetic data exhibited different energy barriers and frequency factors for different parallel reactions. This, in turn, yielded different values of rate constant for different reaction pathways. Such a phenomenon can be used to channel the chlorine in the PVC towards the direct chlorination of $ZnFe_2O_4$ instead of it being released as HCl which would subsequently be captured by Fe_3O_4 (reduced from Fe_2O_3) to form $FeCl_2/FeCl_2 \cdot 2H_2O$. Moreover, since the reduction of Fe_2O_3 by H_2 is kinetically slow, the chlorination selectivity of zinc over iron can be

Table 6

Kinetic parameters associated with the polyene thermal cracking of ZF-PVC mixture (Fig. 3).

Conversion, α	KAS		Friedman			Linear model fitting		
	Activation energy, kJ/mol	Frequency factor, $\ln(A)^a$	Activation energy, kJ/mol	$\ln(A.f(X))$	Frequency factor, $\ln(A)^a$	Activation energy, kJ/mol	Frequency factor, $\ln(A)^a$	f(X)
0.1	182.2	27.92	199.6	30.96	30.94	189.8	28.68	3
0.2	191.9	29.60	162.9	24.80	24.58			
0.3	167.6	25.39	99.2	14.54	13.53			
0.4	142.1	20.97	66.4	8.93	7.84			
0.5	117.6	16.72	62.1	8.03	7.10			
0.6	105.7	14.66	75.1	9.92	9.35			
0.7	99.7	13.62	83.2	10.94	10.76			
0.8	95.3	12.85	84.2	10.70	10.93			
0.9	93.3	12.51	76.8	8.97	9.64			
Average ^b	132.8 ± 36.9	19.36 ± 6.40	101.0 ± 44.9	14.20 ± 7.66	13.85 ± 7.78	Did not fit in model		

^a : Unit of frequency factor (A) is min^{-1} ^b : Average = mean ± SD**Fig. 10.** A comparison between experimental and model generated polyene thermal cracking rates of pure PVC (A) and ZF-PVC mixture (B) at heating rates of 10, 30, and 50 °C/min in the conversion range 0.1 – 0.9 (kinetic data from Friedman model).

maximised by operating at temperatures below 260 °C which would leave iron in its stable form Fe_2O_3 . The evidence in this study showed that Fe_2O_3 can be detected by XRD with the complete absence of ZnFe_2O_4 when the pyrolysis was performed at a low temperature (260 °C) suggesting that selectivity can be maximised with proper controlling of the temperature.

6. Future work

While the kinetic parameters extracted in this work can describe the

thermal behaviour of PVC and ZF-PVC accurately, in some cases they might not reflect the chemical/physical processes fundamentally. The values reported here are lumped values which take into account several consecutive/parallel processes. Moreover, to build a model for the kinetic effect of EAFDs of varying composition and chemistries on the thermal degradation of PVC, one needs to study the kinetic effect of the other major EAFD components such as Fe_2O_3 , Fe_3O_4 , PbO , and in some cases MgO . Hence, in future work, the kinetic effect of the other major EAFD components contributing to a model describing the overall effect of these components combined should be addressed. This, in turn, would reflect the effect of EAFDs with different chemistries world-wide on the thermal degradation of PVC.

For now, the extracted kinetic data produced a very good fit when compared with experimental reaction rate suggesting that the extracted kinetic parameters can be used to predict the thermal behaviour of PVC and ZF-PVC at different temperatures.

Declaration of Competing Interest

The authors declare that they have no known competing financial interests or personal relationships that could have appeared to influence the work reported in this paper.

Acknowledgment

The authors would like to thank Sabrin Samad from the Nanoscale and Microscale Research Centre (nmRC) at the University of Nottingham for providing aid with the SEM analysis.

Appendix A. Supporting information

Supplementary data associated with this article can be found in the online version at [doi:10.1016/j.psep.2022.10.028](https://doi.org/10.1016/j.psep.2022.10.028).

References

- Ahmed, O.H., Altarawneh, M., Al-Harashsheh, M., Jiang, Z.-T., Dlugogorski, B.Z., 2018. Recycling of zincite (ZnO) via uptake of hydrogen halides. *Phys. Chem. Chem. Phys.* 20, 1221–1230.
- Akahira, T., Sunose, T., 1971. Res. Report Chiba Inst. Technol. Sci. Technol 16, 22.
- Al-harashsheh, M., Kingman, S., Al-Makhadmah, L., Hamilton, I.E., 2014. Microwave treatment of electric arc furnace dust with PVC: dielectric characterization and pyrolysis-leaching. *J. Hazard. Mater.* 274, 87–97.
- Al-Harashsheh, M., 2017. Thermodynamic analysis on the thermal treatment of electric arc furnace dust-PVC blends. *Arab. J. Sci. Eng.* 1–13.
- Al-Harashsheh, M., Al-Otoom, A., Al-Makhadmah, L., Hamilton, I.E., Kingman, S., Al-Asheh, S., Hararah, M., 2015. Pyrolysis of poly(vinyl chloride) and—electric arc furnacedust mixtures. *J. Hazard. Mater.* 299, 425–436.
- Al-Harashsheh, M., Aljarrah, M., Al-Otoom, A., Altarawneh, M., Kingman, S., 2018. Pyrolysis kinetics of tetrabromobisphenol A (TBBPA) and electric arc furnace dust mixtures. *Thermochim. Acta* 660, 61–69.

- Al-Harashsheh, M., Altarawneh, S., Al-Omari, M., Altarawneh, M., Kingman, S., Dodds, C., 2021a. Leaching behavior of zinc and lead from electric arc furnace dust–poly (vinyl chloride) residues after oxidative thermal treatment. *J. Clean. Prod.* 328, 129622.
- Al-Harashsheh, M., Orabi, Y., Al-Asheh, S., 2021b. Comparative study on the pyrolysis and leachability of washed/unwashed electric arc furnace dust-PVC mixtures and their residues. *J. Environ. Chem. Eng.*, 105410
- Al-Harashsheh, M., Altarawneh, S., Al-Omari, M., 2022. Selective dissolution of zinc and lead from electric arc furnace dust via oxidative thermolysis with polyvinyl chloride and water-leaching process. *Hydrometallurgy*, 105898.
- Al-Makhadmeh, L.A., Batiha, M.A., Al-Harashsheh, M.S., Altarawneh, I.S., Rawadieh, S.E., 2018. The effectiveness of Zn leaching from EAFD using caustic soda. *Water Air Soil Pollut.* 229, 33.
- Altarawneh, S., Al-Harashsheh, M., Dodds, C., Buttress, A., Kingman, S., 2021. Thermal degradation kinetics of polyvinyl chloride in presence of zinc oxide. *Thermochim. Acta*, 179105.
- Bale, C.W., Chartrand, P., Degterov, S.A., Eriksson, G., Hack, K., Ben Mahfoud, R., Melançon, J., Pelton, A.D., Petersen, S., 2002. FactSage thermochemical software and databases. *Calphad* 26, 189–228.
- Bale, C.W., Bélisle, E., Chartrand, P., Decterov, S.A., Eriksson, G., Gheribi, A.E., Hack, K., Jung, I.H., Kang, Y.B., Melançon, J., Pelton, A.D., Petersen, S., Robelin, C., Sangster, J., Spencer, P., Van Ende, M.A., 2016. Reprint of: FactSage thermochemical software and databases, 2010–2016. *Calphad* 55, 1–19.
- Blazso, M., Jakab, E., 1999. Effect of metals, metal oxides, and carboxylates on the thermal decomposition processes of poly (vinyl chloride). *J. Anal. Appl. Pyrolysis* 49, 125–143.
- Coats, A.W., Redfern, J., 1964. Kinetic parameters from thermogravimetric data. *Nature* 201, 68–69.
- Friedman, H.L., 1964. Kinetics of thermal degradation of char-forming plastics from thermogravimetry. Application to a phenolic plastic. *J. Polym. Sci. Part C Polym. Symposia*, 183–195.
- Georgieva, V., Zvezdova, D., Vlaev, L., 2013. Non-isothermal kinetics of thermal degradation of chitin. *J. Therm. Anal. Calorim.* 111, 763–771.
- Havlík, T., Souza, B.Ve, Bernardes, A.M., Schneider, I.A.H., Mišková, A., 2006. Hydrometallurgical processing of carbon steel EAF dust. *J. Hazard. Mater.* 135, 311–318.
- Ji, M., Chen, L., Que, J., Zheng, L., Chen, Z., Wu, Z., 2020. Effects of transition metal oxides on pyrolysis properties of PVC. *Process Saf. Environ. Prot.* 140, 211–220.
- Jordan, K.J., Suib, S.L., Koberstein, J.T., 2001. Determination of the degradation mechanism from the kinetic parameters of dehydrochlorinated poly(vinyl chloride) decomposition. *J. Phys. Chem. B* 105, 3174–3181.
- Kim, S., 2001. Pyrolysis kinetics of waste PVC pipe. *Waste Manag.* 21, 609–616.
- KiranKumar, T., Roy, G.G., 2022. A review on processing of electric arc furnace dust (EAFD) by pyro-metallurgical processes. *Trans. Indian Inst. Met.* 1–12.
- Kissinger, H.E., 1957. Reaction kinetics in differential thermal analysis. *Anal. Chem.* 29, 1702–1706.
- Laubertova, M., Havlik, T., Parilak, L., Derin, B., Trpcvska, J., 2020. The effects of microwave-assisted leaching on the treatment of electric arc furnace dusts (EAFD). *Arch. Metall. Mater.* 65.
- Lee, G.-S., Song, Y.J., 2007. Recycling EAF dust by heat treatment with PVC. *Miner. Eng.* 20, 739–746.
- Levchik, S.V., Weil, E.D., 2005. Overview of the recent literature on flame retardancy and smoke suppression in PVC. *Polym. Adv. Technol.* 16, 707–716.
- Marcilla, A., Beltrán, M., 1995. Thermogravimetric kinetic study of poly(vinyl chloride) pyrolysis. *Polym. Degrad. Stab.* 48, 219–229.
- Meng, T.-T., Zhang, H., Lü, F., Shao, L.-M., He, P.-J., 2021. Comparing the effects of different metal oxides on low temperature decomposition of PVC. *J. Anal. Appl. Pyrolysis* 159, 105312.
- Mersiowsky, I., Stegmann, R., Ejlertsson, J., 1999. Long term behaviour of poly (vinyl chloride) products under soil buried and landfill conditions. *Plast. Rubber Compos.* 28, 321–326.
- Miranda, R., Pakdel, H., Roy, C., Darmstadt, H., Vasile, C., 1999. Vacuum pyrolysis of PVCII: product analysis. *Polym. Degrad. Stab.* 66, 107–125.
- Omran, M., Fabritius, T., Heikkinen, E.-P., 2019. Selective zinc removal from electric arc furnace (EAF) dust by using microwave heating. *J. Sustain. Metall.* 5, 331–340.
- Oustadakis, P., Tsakiridis, P.E., Katsiapi, A., Agatzini-Leonardou, S., 2010. Hydrometallurgical process for zinc recovery from electric arc furnace dust (EAFD): Part I: characterization and leaching by diluted sulphuric acid. *J. Hazard. Mater.* 179, 1–7.
- Ozawa, T., 1965. A new method of analyzing thermogravimetric data. *Bull. Chem. Soc. Jpn.* 38, 1881–1886.
- Pineau, A., Kanari, N., Gaballah, I., 2006. Kinetics of reduction of iron oxides by H₂: Part I: low temperature reduction of hematite. *Thermochim. Acta* 447, 89–100.
- Plastics-Europe, 2021. *Plastics – the Facts 2021*.
- Šesták, J., Berggren, G., 1971. Study of the kinetics of the mechanism of solid-state reactions at increasing temperatures. *Thermochim. Acta* 3, 1–12.
- Sinaga, G., Wismogroho, A., Fitroturokham, A., Kusumaningrum, R., Widayatno, W., Hadiko, G., Amal, M., 2019. The pyrometallurgical recovery of zinc from electric arc furnace dust (EAFD) with active carbon. *IOP Conference Series: Materials Science and Engineering*. IOP Publishing, 012068.
- Starnes, W.H., Ge, X., 2004. Mechanism of autocatalysis in the thermal dehydrochlorination of poly (vinyl chloride). *Macromolecules* 37, 352–359.
- Suetens, T., Klaasen, B., Van Acker, K., Blanpain, B., 2014. Comparison of electric arc furnace dust treatment technologies using exergy efficiency. *J. Clean. Prod.* 65, 152–167.
- Teo, Y.Y., Lee, H.S., Low, Y.C., Choong, S.W., Low, K.O., 2018. Hydrometallurgical extraction of zinc and iron from electric arc furnace dust (EAFD) using hydrochloric acid. *J. Phys. Sci.* 29, 49–54.
- Vyazovkin, S., 2021. Determining preexponential factor in model-free kinetic methods: how and why? *Molecules* 26, 3077.
- Vyazovkin, S., Burnham, A.K., Criado, J.M., Pérez-Maqueda, L.A., Popescu, C., Sbirrazzuoli, N., 2011. ICTAC Kinetics Committee recommendations for performing kinetic computations on thermal analysis data. *Thermochim. Acta* 520, 1–19.
- Vyazovkin, S., Burnham, A.K., Favregeon, L., Koga, N., Moukhina, E., Pérez-Maqueda, L. A., Sbirrazzuoli, N., 2020. ICTAC Kinetics Committee recommendations for analysis of multi-step kinetics. *Thermochim. Acta* 689, 178597.
- Yakornov, S.A., Pan'shin, A.M., Kozlov, P.A., Ivakin, D.A., 2017. Development of charge pelletizing technology based on electric arc furnace dust for pyrometallurgical processing in rotary kilns. *Metallurgist* 61, 529–534.
- Ye, L., Li, T., Hong, L., 2021. Co-pyrolysis of Fe₃O₄-poly (vinyl chloride)(PVC) mixtures: mitigation of chlorine emissions during PVC recycling. *Waste Manag.* 126, 832–842.
- Ye, Q., Li, G., Peng, Z., Augustine, R., Pérez, M.D., Liu, Y., Liu, M., Rao, M., Zhang, Y., Jiang, T., 2020. Microwave-assisted self-reduction of EAF dust-biochar composite briquettes for production of direct reduced iron. *Powder Technol.* 362, 781–789.
- Yu, J., Sun, L., Ma, C., Qiao, Y., Yao, H., 2016. Thermal degradation of PVC: a review. *Waste Manag.* 48, 300–314.
- Zhang, B., Yan, X.-Y., Shibata, K., Uda, T., Tada, M., Hirasawa, M., 2000. Thermogravimetric-mass spectrometric analysis of the reactions between oxide (ZnO, Fe₂O₃ or ZnFe₂O₄) and polyvinyl chloride under inert atmosphere. *Mater. Trans. JIM* 41, 1342–1350.
- Zhang, M., Li, J., Zeng, Q., Mou, Q., 2019. An experimental study on the reduction behavior of dust generated from electric arc furnace. *Appl. Sci.* 9, 3604.